Open-Delta SBC: a New Converter Topology with Low Number of Sub-Modules for MV applications

D. Lanzarotto[1], P.B Steckler[1], K.Vershinin[1], F. Morel[1]
[1]Supergrid Institute
23 Rue Cyprian,
69100 Villeurbanne, France
E-Mail: damiano.lanzarotto@supergrid-institute.com, pierre-baptiste.steckler@supergrid-institute.com, konstantin.vershinin@supergrid-institute.com, florent.morel@supergrid-institute.com
URL: https://www.supergrid-institute.com/

Keywords

«Medium voltage converter», «AC-DC converter», «DC-AC converter», «Volume reduction», «Modular Multilevel Converters (MMC)»

Abstract

Medium voltage direct current (MVDC) technology has been experiencing a great boom of interest in recent years. This paper aims at giving a contribution to this field by proposing a new converter topology for MVDC applications. This topology is characterized by a low number of sub-modules (SMs) which is strongly related to the converter footprint and complexity. The new topology sizing is compared to the modular multilevel converter (MMC) for the same requirements to highlight advantages and disadvantages of the proposed solution.

Introduction

It is well established nowadays that high voltage direct current (HVDC) technology represents the most advantageous technical solution to problems such as long-distance energy transmission, asynchronous AC systems interconnection, interconnection of different regions requiring submarine and underground cables and transmission of offshore wind power to shore [1, 2]. In particular, the installation of HVDC lines is rapidly expanding in Europe and China. This is driven by the possibility of interconnecting large renewable energy sources located far away from where the main loads are [3-5].
The modular multilevel converter (MMC) represents the standard in terms of converter choice for recent HVDC applications mainly because its advantages compared to line-commuted converters (LCC): capability of realizing an independent P/Q control and small footprint due to the absence of any filter requirements. In addition, its modularity allows the use of low voltage building blocks to create high voltage stacks instead of using hundreds of high frequency switches connected in series. However, if compared to the traditional two-level voltage source converter (VSC), the MMC with half-bridge (HB) sub-modules (SM) requires twice the number of switches for the same output voltage [6] and a large overall converter capacitance leading to higher footprint and costs.
To address the issues mentioned above, researchers have been proposing new hybrid converter topologies with the aim of combining the advantages of the two-level VSC and the modular technology in a single architecture. Many solutions have been proposed following this line of research. The most significant ones consist of: the alternate arm converter (AAC) [7, 8], the series bridge converter (SBC) [9, 10], the hybrid series converter (HSC) [11] and the H-bridge hybrid multilevel converter [12].
Similar reasons to the ones that led to a rapid expansion of HVDC applications have recently started to drive the development of new medium voltage direct current (MVDC) concepts for power distribution [13, 14] with slightly different requirements (range of dc voltage and power of course, but also shape of required PQ domain). For applications with dc voltage of several tens of kV, MMC is an attractive solution thanks the converter modularity and low switching losses (if compared to two or three-level VSCs). Also, the know-how and technology transfer from the HVDC world allows a rapid growing of the number of applications of MMCs in MV domain. However, the above-mentioned weaknesses of MMCs in HVDC applications also arise MVDC then pushing research on alternative modular converters.
The goal of this paper is therefore to propose and analyze a new converter topology has the advantage of a reduced number of SMs in MVDC applications.

The paper is organized as follows. Section 1 deals with the description of the new converter topology, the strategies to balance the internal energy and its characteristic equations. Section 2 presents assumptions made to carry out the converter sizing, defines the key performance indicators (KPIs) and gives the sizing results themselves. Finally section 3 illustrates the comparison between the proposed topology and the MMC in a typical MVDC application.

Open-Delta SBC

General Description

The proposed converter (Figure 1) has been proposed in [15] and is named "open-delta SBC". This new topology consists of two phase-legs, or phase elements (PEs), similar to the ones found in conventional SBC, but there are only two single-phase transformers connected in open delta configuration. Each phase leg consists of a main H-bridge (MHB) and two stacks of SMs: Series Full Bridge (SFB) and Chain Link (CL). A SM stack is simply a series connection of a certain number of SMs which can be of the half-bridge (HB) or full-bridge (FB) type as shown in Figure 2. In particular, in this paper the SFB is a stack composed by HB and FB SMs while the CL in only composed by HB SMs. The voltage created by the stack is given instant by instant by the number of capacitors that are inserted in the circuit and it is characterized by the typical "staircase" profile. In order to create a symmetric and balanced load/generator from the grid standpoint, currents and voltages have to be properly controlled by both phase elements (PE1 and PE2 in Figure 1) as detailed in the following section.

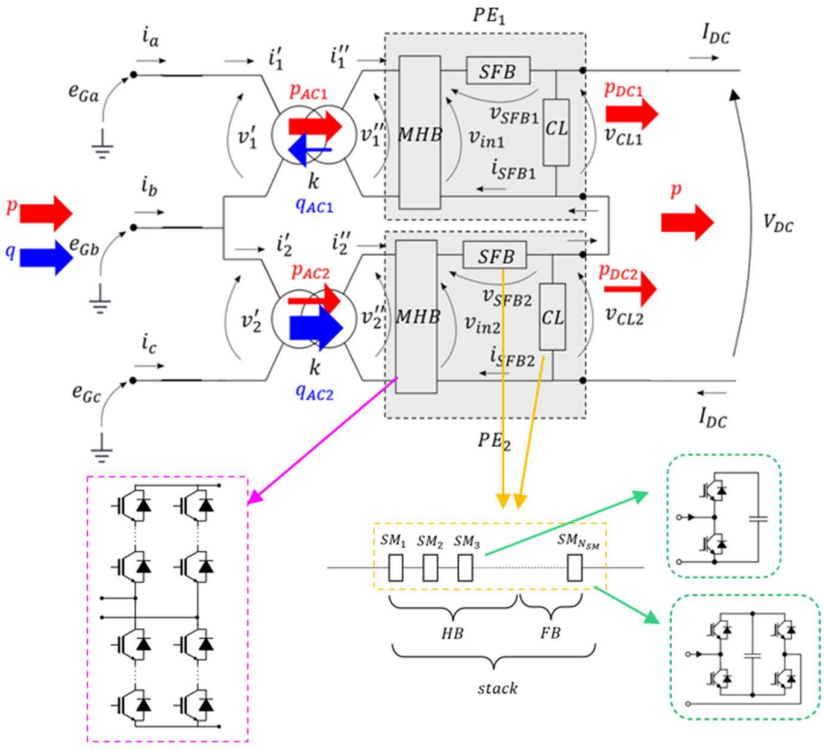

Figure 1 Open-delta SBC topology

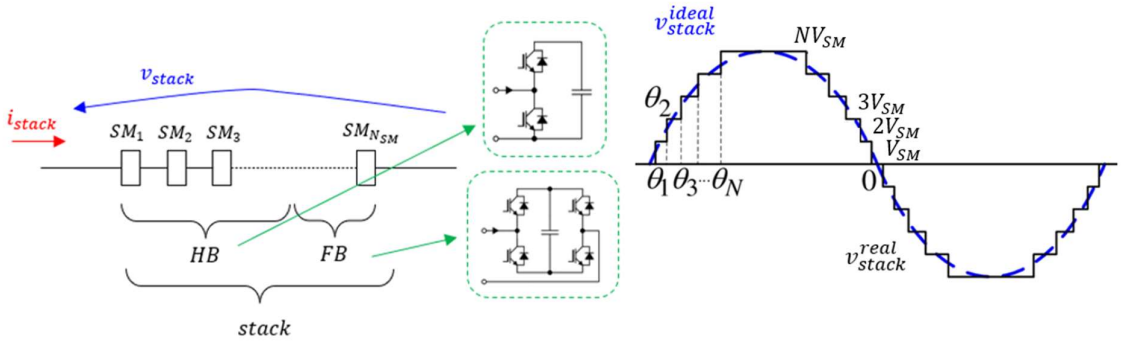

Figure 2 General sub-module stack consisting of both HB and FB SM

Operating Principle

In order to form a symmetric and balanced three-phase system, the open-delta current and voltage vector diagram must be the one of Figure 3 [15], In particular, the converter control must always ensure that:

$$\begin{cases} v_1' = e_{Ga} - e_{Gb} \\ v_2' = e_{Gb} - e_{Gc} \end{cases} \tag{1}$$

where the voltage drop due to the transformer leakage inductance and resistance is neglected. By satisfying (1) we obtain a 3-phase symmetric system, i.e.:

$$\begin{cases} i_1' = i_a \\ i_2' = -i_c \end{cases} \tag{2}$$

Hence, satisfying (2) in the normal operation implies that the two phases of the converter absorb currents which are always of the same amplitude and have a 60 degrees angle difference. Alternatively, if needed, currents with an inverse component can be created. It appears clear that the two phases carry the same amount of active power only when the reactive power is zero (i.e. when φ=0).

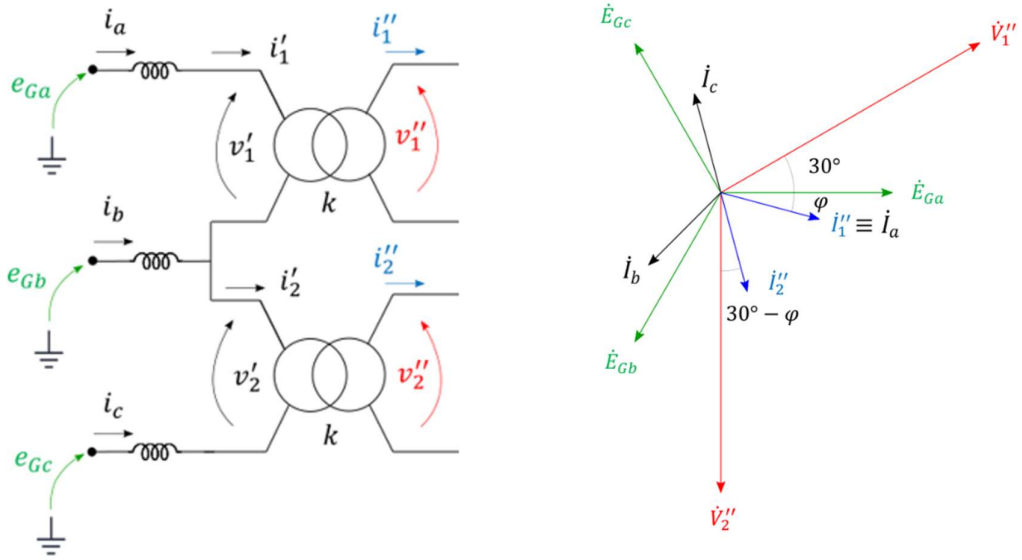

Figure 3 Open-delta connection voltage and current phasor diagram

Given the presence of SM stacks in the converter, the energy balance management issue acquires great importance. As a matter of fact, controlling and maintaining constant the average energy stored in the SM capacitors is crucial for converters with modular elements.

The basis V_b, I_b in Eq. (3) and $P_b = V_b I_b$ are used in the following in order to carry out calculations in per unit (pu).

$$V_b = V_{DC} \quad , \quad I_b = I_{DC,\max} \tag{3}$$

It can be easily verified that with reference to Figure 1 active and reactive powers in phase elements can be written as in Eq (4) where p and q are the active and reactive power absorbed from the grid in per unit (pu), $p_{AC1}, q_{AC1}, p_{AC2}$ and q_{AC2} are the active and reactive power flowing through phase 1 and 2 respectively, as shown in Figure 1.

$$p_{AC1} = \frac{3p - \sqrt{3}q}{6} \quad , \quad q_{AC1} = \frac{\sqrt{3}p + 3q}{6} \quad , \quad p_{AC2} = \frac{3p + \sqrt{3}q}{6} \quad , \quad q_{AC2} = \frac{-\sqrt{3}p + 3q}{6} \tag{4}$$

Energy management

Energy management of the converter and individual stacks is an essential aspect of the MMC converters. For individual stacks voltage and current waveforms observed shall result in zero power variation across fundamental cycle. For initial analysis of the topology presented in this paper we assume that appropriate control system is designed and ignore discrete nature of the voltage across the stack. Therefore, we can use analytical expressions for voltage and current across different elements of the converter.

There is a number of different ways how the converter can operate. In this paper we propose the following operation strategy for the converter which based on the minimizing of the circulating current, which is normally linked to the stack oversizing. In order to do so the CL1 and CL2 voltage are chosen to be time-constant equal to v_{DC1} and v_{DC2}. Considering that DC current is the same in both phase elements and $p_{DC1} = p_{AC1}$ and $p_{DC2} = p_{AC2}$, v_{CL1} and v_{CL2} can be expressed as:

$$v_{DC1} = \frac{p_{AC1}}{p} = \frac{3p - \sqrt{3}q}{6p} \quad , \quad v_{DC2} = \frac{p_{AC2}}{p} = \frac{3p + \sqrt{3}q}{6p} \tag{5}$$

In general, $p_{AC1} \neq p_{AC2}$ and v_{CL1} and v_{CL2} have to adapt to converter set point while their sum always has to be equal to v_{DC}. It is easy to verify from (5) that one has $v_{DC1} = v_{DC2} = 0.5$ at $\cos(\varphi) = 1$, whereas for $\cos(\varphi) = 0.95$ one obtains $v_{DC1} = 0.5 \pm 10\%$ and $v_{DC2} = 0.5 \mp 10\%$. Making the converter operate at lower power factors would further increase the max v_{DC1} and v_{DC2} determining a disadvantageous sizing. This is one of the reasons why the proposed converter is analyzed for MVDC applications, where the minimum $\cos(\varphi)$ is fixed to a certain value close to one (typically in the range 0.9-0.95) [14] leading to a cone-shaped domain in the PQ plane.

By choosing the phase element DC voltage according to (5), the overall energy of each phase element is balanced, therefore if the SFB energy is balanced than CL energy will also be balanced.

Equation (5) describes the CL steady state voltage and current (without loss of generality only the CL1 is considered).

$$\begin{cases} v_{CL1}(t) = v_{DC1} \\ i_{CL1}(t) = i_{SFB1}(t) - i_{DC} \end{cases} \tag{6}$$

By eliminating any harmonic voltage injection (i.e. by choosing that $v_{CL1} = v_{DC1}$ and $v_{CL2} = v_{DC}$), the only way to control the energy stored in the SFB is through the control of the average value of the SFB current. This can be obtained by the selection of an appropriate instant at which the MHB rectifies the transformer secondary side current and voltage. This particular instant depends on the operating condition, and it can be measured by an angle α quantifying its delay from the voltage zero crossing instant. The rectifying action above described is depicted in Figure 4. The part on the left of the figure shows the typical voltage and current waveforms of the MHB in the well-known SBC, where the voltage is rectified at its zero crossing.

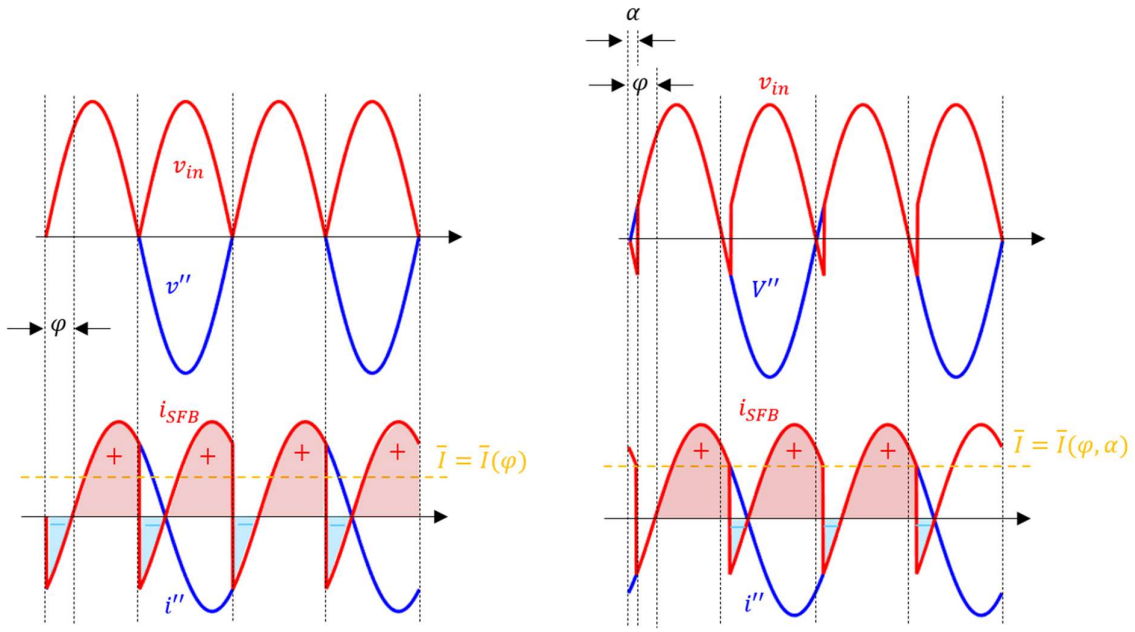

Figure 4 MHB average current control

The part on the right on the other hand shows that the voltage is rectified at an angle α measured from the zero crossing. Thanks to this technique the average value of the SFB current can be controlled. Considering PE1 only without the loss of generality voltage and current in SFB can be expressed as :

$$\begin{aligned} v_{in1} &= \sqrt{2}V''\sin(\omega t)\cdot sign\left[\sin(\omega t+\alpha_1)\right] \\ i_{SFB1} &= \sqrt{2}I''\sin\left(\omega t-\frac{\pi}{6}-\varphi\right)\cdot sign\left[\sin(\omega t+\alpha_1)\right] \end{aligned} \tag{7}$$

$$p_{SFB1} = (v_{in1} - v_{DC1})\, i_{SFB1} = p_{AC1} - v_{DC1} i_{SFB1} \tag{8}$$

where p_{SFB1} is the instantaneous power flowing into the SFB. Therefore, by averaging (8) over the period:

$$P_{SFB1} = \frac{1}{T}\int_0^T p_{SFB1}\,dt = P_{AC1} - v_{DC1}\overline{i_{SFB1}^{pu}}(\varphi, \alpha_1) \tag{9}$$

where P_{AC1} is the active power flowing into PE1 and $\overline{i_{SFB1}^{pu}}(\varphi, \alpha_1)$ is the mean value of the SFB current which depends on φ and α_1. Thus, in order to always maintain the SFB in energy balance, i.e. $P_{SFB1} = 0$, the following relation must always hold:

$$\overline{i_{SFB1}^{pu}} = \frac{P_{AC1}}{v_{DC1}} \tag{10}$$

It is important to remark that the MHB voltage rectified with angle $\alpha \neq 0$ becomes negative (see Figure 4), thus, a slight constructive modification has to be applied on the MHB itself in order to ne able to sustain it. Therefore, a certain amount of switches able to block a certain negative voltage are added as shown in Figure 5. In particular, it can be easily shown that the amount of the negative voltage to block depends on the minimum power factor ($\cos(\varphi)$) for which the converter has to be designed to operate (the lower the $\cos(\varphi)$ the higher is the absolute value of the negative voltage). For instance, with a minimal power factor of 0.95, the maximal negative voltage is roughly 25% of the maximal positive voltage. Thus, the number of the additional necessary switches in the MHB can be calculated. Limiting the power factor to a minimum value allows to not oversize the MHB for the reason explained above, the CL for reasons that can be found in equation (5) and consequently the SFB. This is another reason for the limitation of the converter work points in a cone-shaped PQ plane (MVDC applications) as already mentioned above.

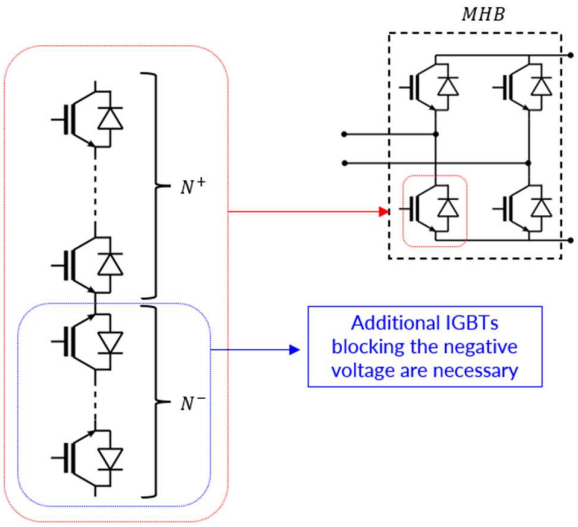

Figure 5 Additional IGBTs and diodes allowing the MHB to operate with negative v_{in} voltages.

Converter Steady State First Harmonic Equations

Summing up, the converter equations in p.u. for the MHB, the CL and the SFB can be expressed as:

$$\begin{cases} v_{in1} = R_v \sin(\omega t) \cdot sign\left[\sin(\omega t + \alpha_1)\right] \\ i_{in1} = \sqrt{2} I^{pu} \sin\left(\omega t - \frac{\pi}{6} - \varphi\right) \cdot sign\left[\sin(\omega t + \alpha_1)\right] \end{cases} \quad MHB_1 \quad (11)$$

$$\begin{cases} v_{CL1} = \frac{3p - \sqrt{3}q}{6p} \\ i_{CL1} = \sqrt{2} I^{pu} \sin\left(\omega t - \frac{\pi}{6} - \varphi\right) \cdot sign\left[\sin(\omega t + \alpha_1)\right] - p \end{cases} \quad CL_1 \quad (12)$$

$$\begin{cases} v_{SFB1} = v_{in1} - v_{CL1} \\ i_{SFB1} = i_{in1} \end{cases} \quad SFB_1 \quad (13)$$

where $R_v = \sqrt{2}V''/V_b$ in which $V''$is the rms value of the secondary side voltage of the transformer and $I^{pu} = \sqrt{\frac{2}{3}}\frac{\sqrt{p^2+q^2}}{R_v}$. Voltage, current and stack energy waveforms are shown in the following figures for a particular operating point.

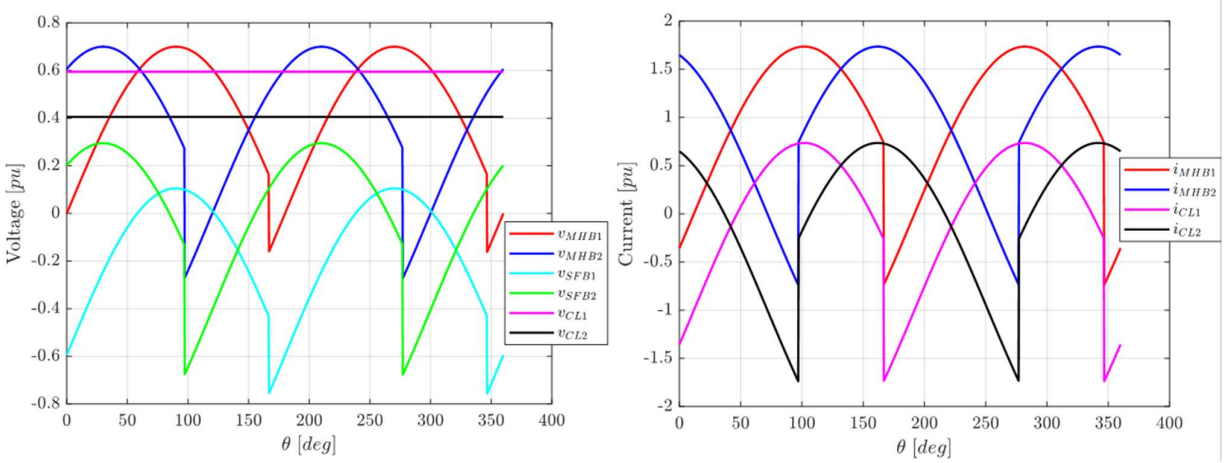

Figure 6 SFB Voltage (left) and current (right) and waveforms for $p = 1$, $cos(\varphi) = 0.95$ and $R_v = 0.7$

Please note that energy unit is time because it is calculated as Joules/Watts, i.e. it is normalized by P_b.

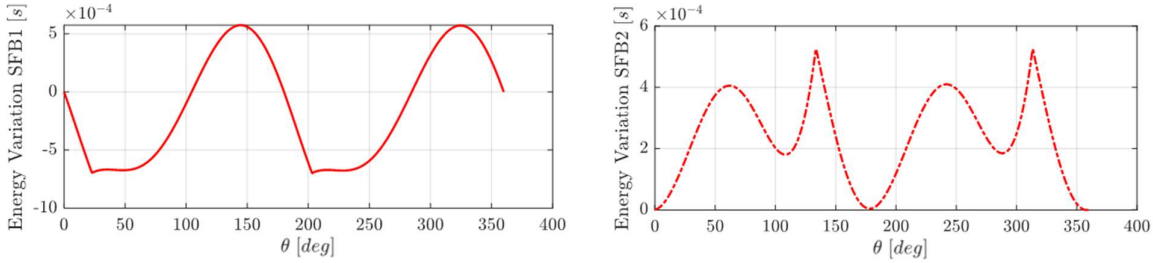

Figure 7 SFB 1 Energy Variation (left) and SFB 2 Energy Variation (right) for $p = 1$, $cos(\varphi) = 0.95$ and $R_v = 0.7$

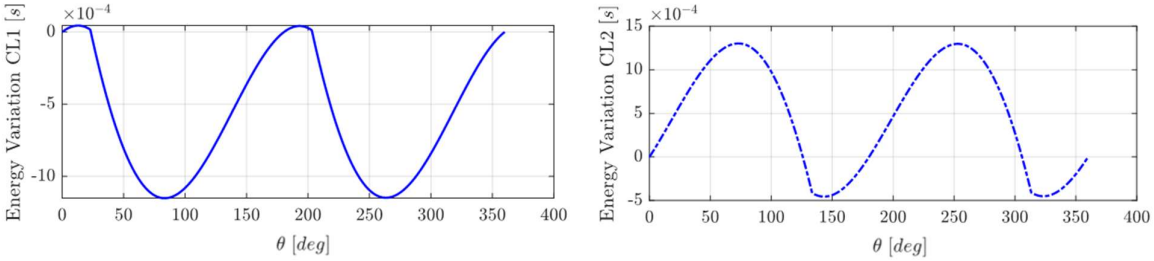

Figure 8 CL1 Energy Variation (left) and CL 2 Energy Variation (right) for $p = 1$, $cos(\varphi) = 0.95$ and $R_v = 0.7$

Sizing results comparison with the MMC

Study case presentation

It is well described in [17] how the interest in a particular converter configuration depends mainly on the converter cost, size and efficiency. It is therefore important to identify parameters able to suitably represent those aspects, consequently, the following key performance indicators (KPIs) are considered here:

- Transformer winding number and transformer sizing power: these parameters are related to the cost and volume of the transformers.
- Switch total sizing power (S_{SW}): it is related to the "quantity of silicon" (voltage to withstand by semiconductors and current passing through them) and therefore related to the converter cost. The total switch sizing power associated to one stack is defined by equation (14).

$$S_{SW}^{stack} = N_{SW}^{stack} V_{\max}^{stack,pu} I_{\max}^{stack,pu} \tag{14}$$

Where N_{SW}^{stack} is the stack switch number and:

$$I_{\max}^{stack,pu} = \max\left\{i_{stack}(t)\right\} / I_{DC,\max} \quad , \quad V_{\max}^{stack,pu} = \max\left\{v_{stack(t)}\right\} / V_{DC} \tag{15}$$

The total converter switch sizing power is obtained by summing the sizing power associated to each stack.

- Stored Energy: this parameter quantifies the energy stored in the converter which is mainly due to SM capacitors which represents the major part of the SM volume. Therefore, this parameter is linked to the to the converter volume.
- Semiconductor switch total sizing power: This is related to the "quantity of silicon" (voltage the semiconductors must withstand and the current passing through them), and therefore is related to the converter cost. In simple terms, it represents the sum of the sizing power of all the switches.
- Sub-module number: it is related to the number of interconnexions between submodules and mechanical assemblies, the number of capacitor voltages to measure, number of discharge circuits (and number of by-pass circuits depending on the manufacturer's technical choices). It is then related to the converter cost.
- Sub-module cell capacitance: it is mainly related to the SM size (which is an important information on the ability to handle it during the construction phase and during replacing operations of faulty SMs). It is also related to the energy stored in an individual sub-module which is a constraint for the devices in the fault courant path in case of SM internal short-circuit. The calculation of the SM capacitance is conducted following the approach described in [18].
- Arm inductor number: it is linked to the converter volume and footprint.

Those KPIs are calculated for the MMC (which represent the state-of-the-art topology) and the open-delta SBC proposed here. The numerical values of the main parameters are listed in table 1 [20].
Thanks to the equations (11), (12) and (13) all the proposed KPIs can be evaluated for the most critical operating point.

Table 1 Numerical values of the main parameters

Name	Symbol	Value
Rated DC power	$P_{DC,max}$	30 MW
DC voltage	V_{DC}	54 kV
P.u. Secondary Voltage	R_v	0.7
Minimum $\cos(\varphi)$	$\cos(\varphi)_{min}$	0.95
Rated SM voltage	$V_{SM,N}$	3.6 kV
Max stack relative voltage variation	δV_{stack}	$\pm 10\%$

Result comparison

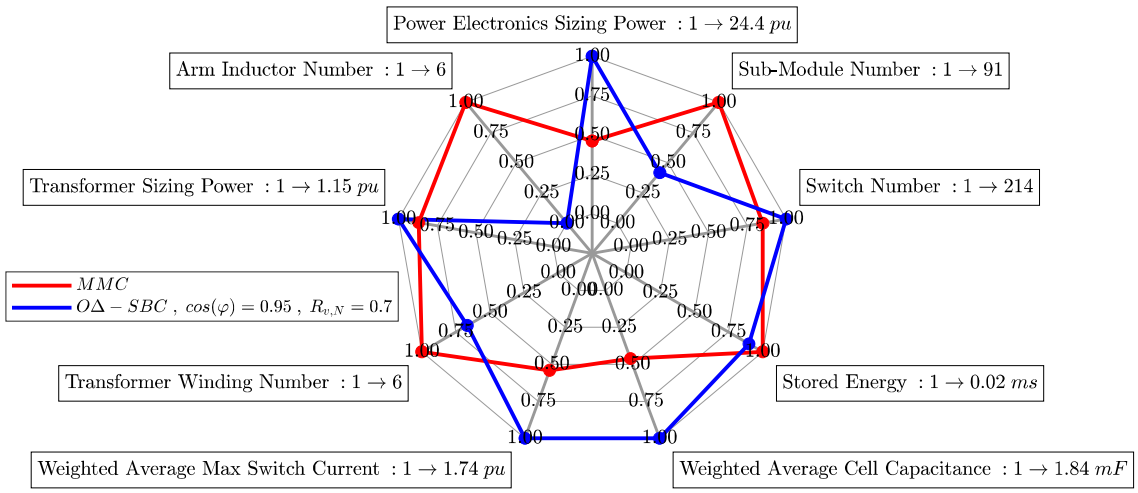

Figure 10 KPI comparison.

For each indicator, the lowest value, the better. Each separate type of KPI is normalized with respect to the maximum of the two to show a relative comparison between the topologies. The notation in the label text corresponding to each KPI: "1→x", means that 1 corresponds to the specified x value. The stored energy unit is time because it is calculated as Joules/Watts, i.e. it is normalized by P_b.

Based on the data presented in Figure 10 it can be seen that open-delta SBC does not have a distinct advantage of the standard configuration of HB MMC. Open-delta SBC has half the number of SM compared to MMC but these submodules are bigger (have larger capacitors and higher switch rated current). Although open delta SBC has slightly lower stored energy it shows much higher semiconductor sizing power.

An improvement in the trade off can be achieved for open-delta SBC if the "DC fault blocking capability" is required by application. In the scope of this paper we consider DC fault blocking capability is an ability of the converter to stay connected to AC grid under existence of the DC pole to pole fault. Indeed, for the MMC, at least 50% of the HB SMs must be replaced by FB SMs for the converter to block DC short-circuits [19]. With reference to for the open-delta SBC, as soon as the fault is detected, the switches in SMs (CLs and SFBs) can be blocked (all IGBTs in SMs controlled to be in off-state, letting only diodes as possible paths for the current) and two strategies can be adopted in order to block the DC fault current.

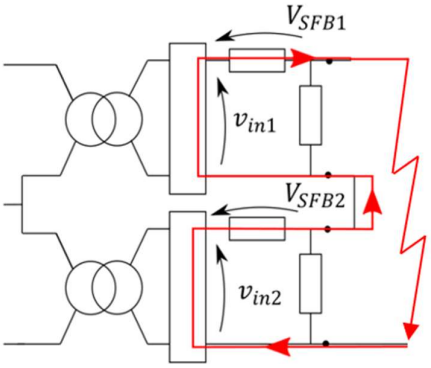

Figure 11 DC short-circuit current path in the open-delta SBC

1. Given the particular structure of the MHB (see Figure 5), it can be designed so that $N^+ = N^-$. Indeed, if the number of diodes pointing downward is the same as the number of diodes pointing upward the DC fault current can be blocked without applying an overvoltage to those devices and their IGBT in parallel.
2. The MHB can be controlled to reproduce the behavior of a diode rectifier when the DC fault occurs (in particular, only the IGBT blocking the negative voltage must be controlled). In this case the SFB voltage ($V_{SFB1,2}$) must be high enough to oppose the MHB output voltage ($v_{in1,2}$) so that the DC current can be taken to zero.

Let us consider the second option . The necessary amount of SFB voltage can be obtained as follows:

$$V_{SFB1} + V_{SFB2} \geq V_{in1} + V_{in2} \tag{16}$$

Assuming $V_{SFB1} = V_{SFB2} = V_{SFB}$ and $V_{in1} = V_{in2} = V_{in}$, then:

$$N_{SM,FB}^{SFB} V_{cell} \geq V_{in} = \sqrt{2} V'' \tag{17}$$

$$N_{SM,FB}^{SFB} \geq \frac{R_v}{V_{cell}^{pu}} \tag{18}$$

Thanks to (18) and to the values chosen in Table 1, one has that $N_{SM,FB}^{SFB} \geq 11$. Since already $N_{FB}^{SFB} = 5$, then 6 HB SMs must be replaced by FB SMs for each SFB. This means that in total $\frac{12}{35} * 100 \cong 34\%$ of the HB SMs must be replaced by FB SMs. Therefore, requiring the DC blocking capability from the open-delta SBC affects less its sizing than the MMC, where at least 50% of SMs must be replaced.

Conclusion

A new converter topology for MVDC applications is investigated. Converter structure principles of operations and energy balancing are briefly described. A set of KPIs are defined and used to assess the advantages and drawbacks of the proposed converter when compared to the MMC for an application case. Results show that the new topology is characterized by a significantly lower SM number with respect to the MMC. It can lead to an advantageous solution from complexity, cost and footprint points of view**.** Moreover, if the converter is required to able to block faults on the DC side, less switches should be added than in the MMC case.

References

[1] M. P. Bahrman and B. K. Johnson, "The ABCs of HVDC transmission technologies," *IEEE power and energy magazine,* vol. 5, pp. 32-44, 2007.

[2] P. Bresesti, W. L. Kling, R. L. Hendriks, and R. Vailati, "HVDC connection of offshore wind farms to the transmission system," *IEEE Transactions on energy conversion,* vol. 22, pp. 37-43, 2007.

[3] X. Qin, P. Zeng, Q. Zhou, Q. Dai, and J. Chen, "Study on the development and reliability of HVDC transmission systems in China," in *2016 IEEE International Conference on Power System Technology (POWERCON)*, 2016, pp. 1-6.

[4] H. Xie, Z. Bie, and G. Li, "Reliability-oriented networking planning for meshed VSC-HVDC grids," *IEEE Transactions on Power Systems,* vol. 34, pp. 1342-1351, 2018.

[5] A. Orths, A. Hiorns, R. van Houtert, L. Fisher, and C. Fourment, "The European North seas countries' offshore grid initiative—The way forward," in *2012 IEEE Power and Energy Society General Meeting*, 2012, pp. 1-8.

[6] M. B. Ghat, S. K. Patro, and A. Shukla, "The hybrid-legs bridge converter: A flexible and compact VSC-HVDC topology," *IEEE Transactions on Power Electronics,* vol. 36, pp. 2808-2822, 2020.

[7] M. M. C. Merlin, D. Soto-Sanchez, P. D. Judge, G. Chaffey, P. Clemow, T. C. Green*, et al.*, "The extended overlap alternate arm converter: A voltage-source converter with DC fault ride-through capability and a compact design," *IEEE Transactions on Power Electronics,* vol. 33, pp. 3898-3910, 2017.

[8] M. M. Merlin, T. C. Green, P. D. Mitcheson, D. R. Trainer, R. Critchley, W. Crookes*, et al.*, "The alternate arm converter: A new hybrid multilevel converter with dc-fault blocking capability," *IEEE transactions on power delivery,* vol. 29, pp. 310-317, 2013.

[9] C. M. Diez, A. Costabeber, F. Tardelli, D. Trainer, and J. Clare, "Control and experimental validation of the series bridge modular multilevel converter for HVDC applications," *IEEE Transactions on Power Electronics,* vol. 35, pp. 2389-2401, 2019.

[10] E. M. Farr, D. R. Trainer, O. E. Idehen, and K. Vershinin, "The series bridge converter (SBC): AC faults," *IEEE Transactions on Power Electronics,* vol. 35, pp. 4467-4471, 2019.

[11] S. K. Patro, A. Shukla, and M. B. Ghat, "Hybrid series converter: a dc fault tolerant HVDC converter with wide operating range," *IEEE Journal of Emerging and Selected Topics in Power Electronics,* 2019.

[12] M. B. Ghat and A. Shukla, "A new H-bridge hybrid modular converter (HBHMC) for HVDC application: operating modes, control, and voltage balancing," *IEEE Transactions on Power Electronics,* vol. 33, pp. 6537-6554, 2017.

[13] P. Le Métayer, J. Paez, S. Touré, C. Buttay, D. Dujic, E. Lamard*, et al.*, "Break-even distance for MVDC electricity networks according to power loss criteria," in *2021 23rd European Conference on Power Electronics and Applications (EPE'21 ECCE Europe)*, 2021, pp. 1-9.

[14] "ANGLE-DC, 2015 Electricity Network Innovation Competition," 2015.

[15] P.-B. Steckler, "Pierre-Baptiste Steckler, PATENT APPLICATION: Convertisseur de tension AC/DC triphasé comprenant uniquement deux modules de conversion électrique, Assignee: SUPERGRID INSTITUTE, FR3112042A1," 2020.

[16] E. Amankwah, A. Costabeber, A. Watson, D. Trainer, O. Jasim, J. Chivite-Zabalza*, et al.*, "The series bridge converter (SBC): A hybrid modular multilevel converter for HVDC applications," in *2016 18th European Conference on Power Electronics and Applications (EPE'16 ECCE Europe)*, 2016, pp. 1-9.

[17] N. Evans, P. Dworakowski, M. Al-Kharaz, S. Hegde, E. Perez, and F. Morel, "Cost-performance framework for the assessment of Modular Multilevel Converter in HVDC transmission applications," in *IECON 2019-45th Annual Conference of the IEEE Industrial Electronics Society*, 2019, pp. 4793-4798.

[18] M. Merlin, T. Green, P. Mitcheson, F. Moreno, K. Dyke, and D. Trainer, "Cell capacitor sizing in modular multilevel converters and hybrid topologies," in *2014 16th European Conference on Power Electronics and Applications*, 2014, pp. 1-10.

[19] P.-B. Steckler, "Contribution à la conversion AC/DC en Haute Tension," Université de Lyon, 2020.

[20] D. Lanzarotto, F. Morel, P.-B. Steckler, and K. Vershinin, “Rapid Evaluation Method for Modular Converter Topologies,” Energies, vol. 15, no. 10, p. 3492, May 2022, doi: 10.3390/en15103492. [Online]. Available: http://dx.doi.org/10.3390/en15103492